PERGAMON

International Journal of Solids and Structures 39 (2002) 175–198

INTERNATIONAL JOURNAL OF SOLIDS and STRUCTURES

www.elsevier.com/locate/ijsolstr

Snap-through of unsymmetric fiber-reinforced composite laminates

M.-L. Dano [a,1], M.W. Hyer [b,*]

[a] *Departement de Genie Civil, Universite LAVAL, Pavillon Adrien-Pouliot Quebec, Quebec, Canada G1K 7P4*

[b] *Department of Engineering Science and Mechanics, Virginia Polytechnic Institute and State University, Blacksburg, VA 24061-0219, USA*

Received 8 September 2000; in revised form 7 March 2001

Abstract

An approximate theory based on assumed strain and displacement fields, the Rayleigh–Ritz technique, and virtual work is used to predict the snap-through forces and moments for three families of unsymmetric fiber-reinforced composite laminates. Unsymmetric laminates generally have two stable equilibrium configurations when cooled from their elevated cure temperature, and it is the moment required to snap the laminate from one stable configuration to the other that is the subject of this paper. A simple force-controlled experiment is described which is used to measure the snap-through moment and the characteristics of the configuration change, by way of strains, in four laminates. The correlation between predicted results and experimental measurements is quite good, both in terms of moment levels and in terms of strain response.

Keywords: Thermally-induced deformations; Stability; Geometrically nonlinear effects; Rayleigh–Ritz technique

1. Introduction and background

At one time the characteristics of unsymmetric polymeric matrix fiber-reinforced composite laminates were nothing more than an unexplained curiosity (Hyer, 1981a). After curing flat at an elevated temperature (Fig. 1a) a thin $[90_4/0_4]_T$ cross-ply unsymmetric graphite-epoxy laminate, for example, will have two cylindrical configurations when cooled to room temperature. One cylindrical configuration has a large curvature in the x-direction and an imperceptible curvature in the y-direction (Fig. 1b). The other cylindrical configuration has a large curvature in the y-direction and an imperceptible curvature in the x-direction (Fig. 1c). The curvatures for the two configurations are of opposite signs and the laminate can be changed from one configuration to the other by a simple snap-through action initiated by applying moments to the edges of the laminate. Subsequent analysis by Hyer (1982) explained this behavior. Obviously, the difference in thermal expansion of the material in the fiber direction relative to the thermal expansion

* Corresponding author. Tel.: +1-540-231-5372; fax: +1-540-231-4574.

E-mail addresses: mldano@gci.ulaval.ca (M.-L. Dano), hyerm@vt.edu (M.W. Hyer).

[1] Tel.: +1-418-656-2131, ext. 8547.

0020-7683/01/$ - see front matter
PII: S0020-7683(01)00074-9

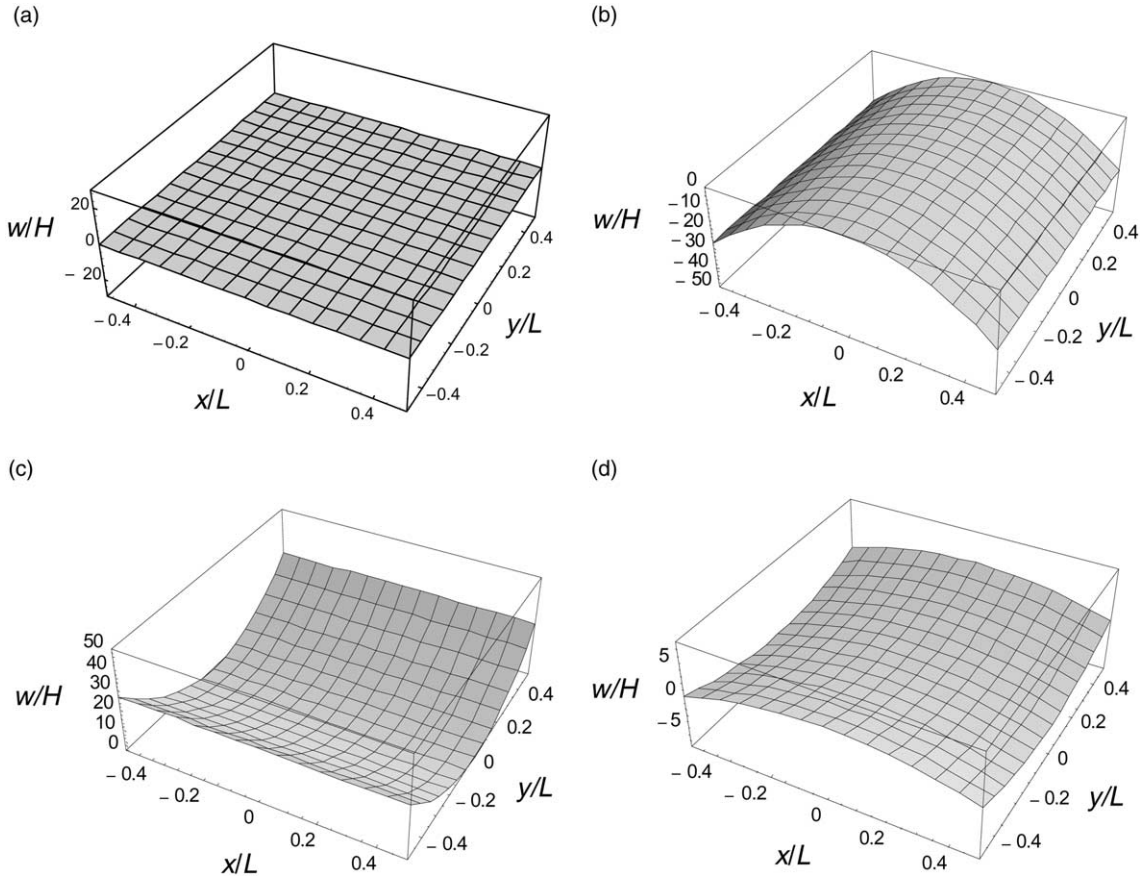

Fig. 1. Shapes of $[90_4/0_4]_T$ laminate. (a) Curing temperature: flat, (b) room temperature: stable cylindrical configuration with curvature in the x-direction, (c) room temperature: stable cylindrical configuration with curvature in the y-direction, and (d) room temperature: unstable saddle configuration.

perpendicular to the fibers is what is responsible for the flat cured laminate deforming as it is cooled. However, as seen by the scale in Fig. 1, with the laminate exhibiting out-of-plane deflections, w, many times the laminate thickness, H, the key to explaining the behavior was inclusion of geometric nonlinearities. The numerical results revealed that in addition to the two cylindrical shapes, a saddle shaped configuration, as shown in Fig. 1d, also satisfies the equilibrium conditions. A stability analysis, however, showed that the saddle shape corresponds to unstable equilibrium and therefore is never observed. The two cylindrical configurations are stable and corresponded to equal minimum total potential energy states. Interestingly, the saddle is the shape predicted when geometric nonlinearities are ignored. Also, thicker unsymmetric laminates exhibit a single saddle shape. Hyer's analysis shows this thickness effect is actually dependent on the side length-to-thickness ratio rather than just the thickness. In a subsequent analysis, Hyer (1982) considered slightly more general cross-ply laminates, e.g., $[0_3/90]_T$. Hamamoto and Hyer (1987) investigated the configurations of cross-ply laminates as they were cooled from their elevated cure temperature. As most composite laminates are cured in an autoclave or hot press, usually within a restraining vacuum bag, they are not free to deform during cooling and also are not visible until cooled to room-temperature conditions and removed from the hot press or autoclave. Therefore, observation during cooling is not really

possible. However, since curing occurs at the elevated temperature and the step of cooling to room temperature is reversible, cured and cooled laminates can be reheated under unrestrained conditions and the deformation behavior measured. Hamamoto and Hyer took this approach and investigated temperature–curvature relations for several laminates. Correlation between predictions and measurements was good.

Dang and Tang (1986) extended Hyer's earlier work to include unsymmetric laminates more general than just the cross-ply case. If the unsymmetric laminate is not a simple cross-ply, it will develop twist curvature, in addition to curvature in the x- and y-directions, as it cools. These curvatures can be interpreted in terms of principal curvatures and principal curvature directions. Dang and Tang introduced more involved polynomial functions than Hyer (1981b) originally used for the approximate displacement fields in their Rayleigh–Ritz formulation, and the principal curvature coordinate system was used as a starting point. Through coordinate transformation, the displacements in the structural coordinate system, a system with the coordinate axes aligned with the side lengths of the laminate, were computed. The total potential energy was formed and the first variation used to obtain equilibrium equations. The assumed polynomial displacement functions were not chosen carefully, as only the sum of two of the unknown coefficients in the assumed functions could be solved for, as opposed to being able to solve for all the unknown coefficients, which is usually the case with a Rayleigh–Ritz approach. None-the-less, comparisons with limited experimental data from Hyer (1981a) were reasonable. Jun and Hong (1990) modified Hyer (1981b) original approximate displacement field by adding more terms in the polynomials to account for the inplane shear strain Hyer assumed was negligible for the cross-ply case. They found that shear strain was indeed negligible for square laminates with very large or very small length-to-thickness ratios. However, for intermediate length-to-thickness ratios, they found shear strain could be important. Jun and Hong (1992) then modified Dang and Tang (1986) approximate displacement functions by adding even more polynomial terms and looking at more general unsymmetric laminates. They obtained fairly complex displacement expressions and used several changes of variables and trigonometric relations to simplify these expressions. The approach seemed unnecessarily complicated, and to verify the theory, a few experimental results for principal curvature directions from Hyer (1981a) were used. Later, Peeters et al. (1996) developed a theory for square angle-ply laminates based on the work of Jun and Hong (1992) by modifying their displacement functions. The modified displacement functions used a more complete set of third-order polynomials. To compute the total potential energy, Peeters et al. fixed the value of the principal curvature direction, assuming it was 45° relative to the laminate edges for all laminates in their study. This assumption, presumably, was based on the linear theory which predicts that angle-ply laminates exhibit equal curvatures in the x- and y-directions and therefore have the principal curvature direction equal to 45°. Other constraints were applied as part of their theory, and experimental results from one 30° angle-ply laminate were presented to compare with the theoretical model. The comparisons between the experiment and predictions were reasonable, though the authors went on to explain how manufacturing problems, material property uncertainties, and material inhomogeneities could have influenced the experimental results. Cho et al. (1998) revisited the earlier work of Hyer (1981a,b, 1982) by assuming that slippage between the tool plate and the laminate during cure and cooling are a factor in the room-temperature curvature observed. They provided numerical and experimental evidence that slippage can be a factor, accounting for at least a 25% reduction in curvature as compared to the case were slippage is ignored. Though they began the analysis for general laminates by using transformations much like Jun and Hong (1990, 1992), results centered on cross-ply laminates.

There have been a number of finite-element analyses of unsymmetric laminates, most notably Schlecht et al. (1995, 1999). This approach can, of course, be applied to general problems and issues can be studied in more detail. However, the approach can lead to difficulties finding multiple solutions and dealing with unstable equilibrium configurations. Often, constraints have to be applied to the finite-element model to force a particular solution in a situation where there are multiple solutions. Of course, something must be

known about these other solutions, including whether or not they exist. Tuttle et al. (1996) exploited the original theory by Hyer (1981b) to study the influence of fiber pre-stress on residual curing stresses.

More recently, Dano and Hyer (1997) developed a fairly comprehensive theory for general unsymmetric laminates. As the total potential energy does not explicitly involve displacements, and since for the cooling problem there is no agent to do external work, Dano and Hyer's development centered on approximations to the strains. In addition, unlike previous analyses for general unsymmetric laminates, the analysis was developed in the structural coordinate system rather than the principal curvature coordinate system. If the latter approach is taken, then the orientation of the principal curvature coordinate system relative to the side lengths of the laminate is an unknown and must be solved for. The orientation appears in the ensuing algebra in transcendental fashion, making calculations difficult. Peeters et al. made a priori assumptions about the orientation in order to avoid the algebra but, as shown by Dano and Hyer (1997), their assumption was not correct. Dano and Hyer (1997) used polynomial expressions for the strains and studied three families of unsymmetric laminates. Curvatures were measured in the structural coordinate system for eight laminates from these families. The data were transformed into principal curvatures and principal curvature directions, and these were compared with predictions. Good agreement was obtained.

2. Present paper

As the snapping from one configuration to another is a very interesting aspect of unsymmetric laminates, the present paper focuses on snap through. It is felt there could be useful applications for unsymmetric laminates in situations where multiple structural configurations are needed. Rather than continuously expending energy to force a structure with a single configuration to maintain an alternative configuration, as is currently done with a number of so-called smart structure concepts, expending energy for a short period of time to force a structure to change from one natural and stable configuration to another natural and stable configuration would seem to be a more energy-efficient, predicable, and reliable approach. As such, the snap-through event, and in particular, the snap-through forces or moments, become important. Dano and Hyer (1996) briefly looked at the snap-through phenomenon for a specific cross-ply laminate. They predicted and measured the forces in a loading scheme designed to exert known moments near the edges of a cross-ply laminate and found good correlations with predicted force vs. strain relations. In their finite-element analysis, Schlecht and Schulte (1999) held the center point of the laminate and computed the corner forces necessary to effect snap through from one cylindrical configuration to the other. It was shown that the for $[0_2/\theta_2]_T$ laminates the force required to produce snapping increases monotonically with θ.

The present paper builds on the approach of Dano and Hyer (1996), which was restricted to cross-ply laminates, and presents further experimental data. This paper begins by developing the theory necessary to compute the moments, actually forces acting through moment arms, necessary to cause general unsymmetric laminates to change configurations. The Rayleigh–Ritz technique is used in conjunction with the principle of virtual work. After the theory is presented, numerical results for a number of laminates are presented. Then, experiments are described which are used to measure the snap-through forces. Finally, comparisons between measurements and numerical results for four laminates are presented. Snap-through force levels and strain characteristics are discussed.

3. Problem formulation

Fig. 2a shows an overall view of the scheme considered here to produce snap through. At the cure temperature the laminate is flat, the x- and y-directions are parallel with the orthogonal edges of the flat rectangular laminate, and the z-direction is perpendicular to the laminate. (The x-, y-, and z-directions are considered the structural coordinates.) When cooled to room temperature, since the laminate is generally

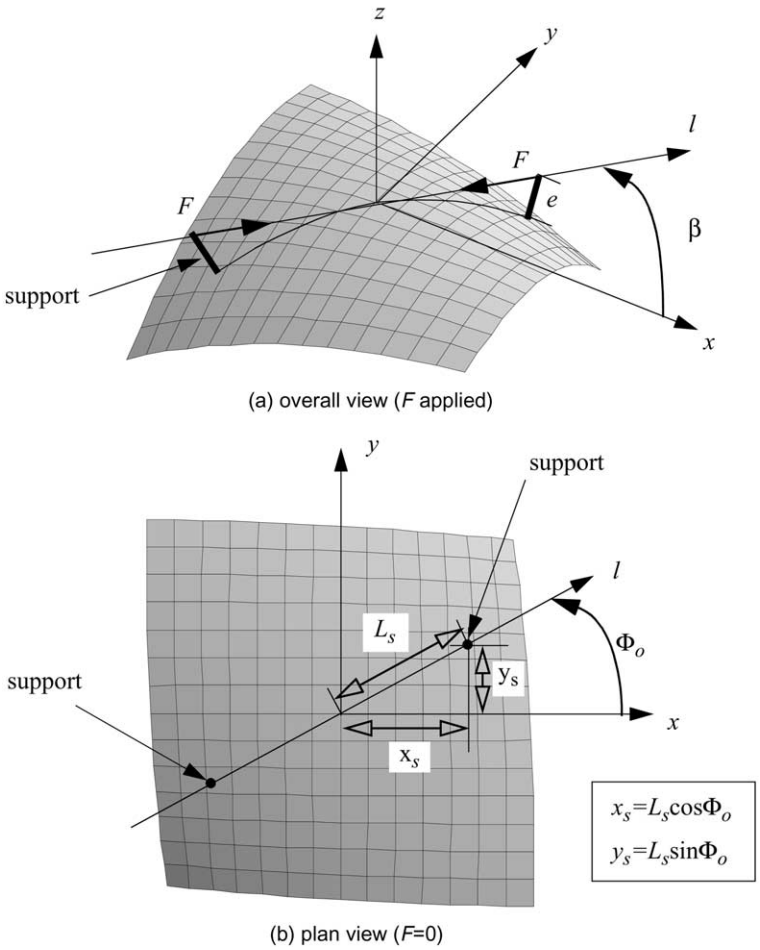

Fig. 2. Geometry of the force arrangement.

unsymmetric, as opposed to being a cross- or angle-ply laminate, the shape of the laminate consists of curvatures in the x- and y-directions as well as twist curvature, as is shown in Fig. 2a. To affect a snap through, it will be assumed that supports of length e are attached perpendicular to the laminate and forces F are applied at the upper ends of the supports to generate moments on the laminate. The forces on the ends of the two supports are collinear and directed toward each other. While this approach may seem rather contrived, the set-up lends itself to relatively simple experiments and conceivably, to continue with the discussion of smart structures, the force could be generated by a shape memory alloy wire stretched between the tips of the supports and heated so as to change phase and contract. Moreover, as snapping back and forth from one configuration to another may be desirable, a companion set of supports and wires may be attached on the underside of the laminate to affect the reverse snap. This companion set will not be considered here. It could be argued that such an arrangement of supports and wires might be cumbersome. No doubt, variants can be designed which make the arrangement more tidy, but that is not the issue here. In Fig. 2a the angle β corresponds to the angle between the line of action of the forces, denoted by l, and the x-direction. The bases of the supports are attached so that initially the line of action of the forces is in a principal curvature direction of the room-temperature configuration of the laminate. The principal

curvature direction makes angle Φ_0 with the $+x$-axis and Fig. 2b shows a planform view of the scheme when $F = 0$. The coordinates of where the bases of the supports attach to the laminate are denoted x_s and y_s, and the distance between the bases of the supports is $2L_s$, these being measured when the laminate is flat. The relation between these geometric quantities is

$$\begin{aligned} x_s &= \pm L_s \cos \Phi_0, \\ y_s &= \pm L_s \sin \Phi_0. \end{aligned} \tag{1}$$

The forces exert moments on the laminate proportional to F and e. The response of the laminate to these moments will be determined using the principle of virtual work, which can be stated as

$$\delta W_{\mathrm{T}} = \delta \Pi - \delta W_F = 0, \tag{2}$$

where δW_{T} is the total virtual work, $\delta \Pi$ the first variation of the strain energy, and δW_F the virtual work of the applied forces.

3.1. Formulating $\delta \Pi$

Assuming a state of plane stress, the strain energy of the laminate, Π, can be expressed as a function of the material and geometric properties of the laminate, the applied temperature change, ΔT, and the total strains by,

$$\begin{aligned} \Pi = \int_{\frac{-L_x}{2}}^{\frac{L_x}{2}} \int_{\frac{-L_y}{2}}^{\frac{L_y}{2}} \int_{\frac{-H}{2}}^{\frac{H}{2}} \Big(& \tfrac{1}{2}\bar{Q}_{11}\varepsilon_x^2 + \bar{Q}_{12}\varepsilon_x\varepsilon_y + \bar{Q}_{16}\gamma_{xy}\varepsilon_x + \tfrac{1}{2}\bar{Q}_{22}\varepsilon_y^2 + \bar{Q}_{26}\gamma_{xy}\varepsilon_y + \tfrac{1}{2}\bar{Q}_{66}\gamma_{xy}^2 - (\bar{Q}_{11}\alpha_x + \bar{Q}_{12}\alpha_y \\ & + \bar{Q}_{16}\alpha_{xy})\varepsilon_x \Delta T - (\bar{Q}_{12}\alpha_x + \bar{Q}_{22}\alpha_y + \bar{Q}_{26}\alpha_{xy})\varepsilon_y \Delta T - (\bar{Q}_{16}\alpha_x + \bar{Q}_{26}\alpha_y + \bar{Q}_{66}\alpha_{xy})\gamma_{xy}\Delta T \Big) \, \mathrm{d}x \, \mathrm{d}y \, \mathrm{d}z, \end{aligned} \tag{3}$$

where the Q_{ij} terms are the transformed reduced stiffnesses of the individual layers (Hyer, 1998), and L_x and L_y are the planform dimensions when the laminate is flat. The total strains $\varepsilon_x, \varepsilon_y, \gamma_{xy}$ are given by,

$$\varepsilon_x = \varepsilon_x^0 + z\kappa_x^0 \quad \varepsilon_y = \varepsilon_y^0 + z\kappa_y^0 \quad \gamma_{xy} = \gamma_{xy}^0 + z\kappa_{xy}^0. \tag{4}$$

The quantities $\varepsilon_x^0, \varepsilon_y^0, \gamma_{xy}^0$ and $\kappa_x^0, \kappa_y^0, \kappa_{xy}^0$ are the total midplane strains and curvatures, respectively, defined by

$$\varepsilon_x^0 = \frac{\partial u^0}{\partial x} + \frac{1}{2}\left(\frac{\partial w^0}{\partial x}\right)^2 \quad \varepsilon_y^0 = \frac{\partial v^0}{\partial y} + \frac{1}{2}\left(\frac{\partial w^0}{\partial y}\right)^2 \quad \gamma_{xy}^0 = \frac{\partial u^0}{\partial y} + \frac{\partial v^0}{\partial x} + \frac{\partial w^0}{\partial x}\frac{\partial w^0}{\partial y} \tag{5}$$

$$\kappa_x^0 = -\frac{\partial^2 w^0}{\partial x^2} \quad \kappa_y^0 = -\frac{\partial^2 w^0}{\partial y^2} \quad \kappa_{xy}^0 = -2\frac{\partial^2 w^0}{\partial x \, \partial y}, \tag{6}$$

where $u^0, v^0,$ and w^0 are the displacements of the midplane in the x-, y-, and z-directions, respectively. It is seen in the above equations that geometric nonlinearities in the sense of von Kármán are included. Here the extensional midplane strains are approximated using the following set of complete polynomials:

$$\begin{aligned} \varepsilon_x^0 &= c_1 + c_2 x^2 + c_3 y^2 + c_4 xy, \\ \varepsilon_y^0 &= c_5 + c_6 x^2 + c_7 y^2 + c_8 xy, \end{aligned} \tag{7}$$

where the $c_i, i = 1, 8$ are to-be-determined coefficients. This functional form for the extensional strains has been discussed in Dano and Hyer (1997), where a more general form was used but was found to be unnecessary. Independently, Cho et al. (1998) used identical expressions for extensional strains. The inplane shear strain is more difficult to assume, as it must be consistent with the strains ε_x^0 and ε_y^0. To assure consistent strains, the inplane shear strain is determined using the strain–displacement relations, and that will be done shortly. The out-of-plane displacement w^0 can be easily approximated by

$$w^0(x,y) = \tfrac{1}{2}(c_9x^2 + c_{10}y^2 + c_{11}xy), \tag{8}$$

where c_9,c_{10}, and c_{11} are three more to-be-determined coefficients which represent, respectively, the negative of the curvatures in the x- and y-directions and the negative of the twist curvature, as

$$\kappa_x^0 = -\frac{\partial^2 w^0}{\partial x^2} = -c_9 \quad \kappa_y^0 = -\frac{\partial^2 w^0}{\partial y^2} = -c_{10} \quad \kappa_{xy}^0 = -2\frac{\partial^2 w^0}{\partial x\,\partial y} = -c_{11}. \tag{9}$$

It is seen that the curvatures are predicted to be a constant throughout the laminate. Alternatively, the curvatures c_9, c_{10}, and c_{11} can be thought of as average curvatures. The form of $w^0(x,y)$ in Eq. (8) is felt to represent the out-of-plane displacements for a large percentage, if not all, of the unsymmetric laminates observed.

Using the expressions for the extensional strains ε_x^0 and ε_y^0 and the out-of-plane displacement w^0, the inplane displacements u^0 and v^0 can be determined by integrating the rearranged strain–displacement relations given by

$$\frac{\partial u^0}{\partial x} = \varepsilon_x^0 - \frac{1}{2}\left(\frac{\partial w^0}{\partial x}\right)^2 = c_1 + c_2x^2 + c_3y^2 + c_4xy - \frac{1}{2}\left(c_9x + \frac{1}{2}c_{11}y\right)^2 \tag{10}$$

and

$$\frac{\partial v^0}{\partial y} = \varepsilon_y^0 - \frac{1}{2}\left(\frac{\partial w^0}{\partial y}\right)^2 = c_5 + c_6x^2 + c_7y^2 + c_8xy - \frac{1}{2}\left(c_{10}y + \frac{1}{2}c_{11}x\right)^2. \tag{11}$$

Integrating Eqs. (10) and (11) with respect to x and y leads to, respectively,

$$u^0(x,y) = c_1x + \tfrac{1}{3}c_2x^3 + c_3xy^2 + \tfrac{1}{2}c_4x^2y - \tfrac{1}{6}c_9^2x^3 - \tfrac{1}{4}c_9c_{11}x^2y - \tfrac{1}{8}c_{11}^2xy^2 + h(y) \tag{12}$$

and

$$v^0(x,y) = c_5y + c_6x^2y + \tfrac{1}{3}c_7y^3 + \tfrac{1}{2}c_8xy^2 - \tfrac{1}{6}c_{10}^2y^3 - \tfrac{1}{4}c_{10}c_{11}xy^2 - \tfrac{1}{8}c_{11}^2x^2y + g(x), \tag{13}$$

where $h(y)$ and $g(x)$ are a result of partial integration. To maintain the pattern of $u^0(x,y)$ and $v^0(x,y)$ being polynomials in odd powers of x and y, $h(y)$ and $g(x)$ were chosen to be of the following form:

$$\begin{aligned} h(y) &= c_{12}y + \tfrac{1}{3}c_{13}y^3, \\ g(x) &= c_{15}x + \tfrac{1}{3}c_{14}x^3. \end{aligned} \tag{14}$$

In the above c_{12}, c_{13}, c_{14}, are c_{15} are additional unknown coefficients. To eliminate rigid body rotation in the x–y plane from being part of the assumed displacements, c_{15} has to be equal to c_{12}. Therefore the displacements $u^0(x,y)$ and $v^0(x,y)$ can be simply expressed as

$$\begin{aligned} u^0(x,y) &= c_1x + c_{12}y + \frac{1}{2}\left(c_4 - \frac{1}{2}c_9c_{11}\right)x^2y + \left(c_3 - \frac{c_{11}^2}{8}\right)xy^2 + \frac{1}{3}\left(c_2 - \frac{1}{2}c_9^2\right)x^3 + \frac{1}{3}c_{13}y^3, \\ v^0(x,y) &= c_{12}x + c_5y + \left(c_6 - \frac{c_{11}^2}{8}\right)x^2y + \frac{1}{2}\left(c_8 - \frac{1}{2}c_{10}c_{11}\right)xy^2 + \frac{1}{3}\left(c_7 - \frac{1}{2}c_{10}^2\right)y^3 + \frac{1}{3}c_{14}x^3. \end{aligned} \tag{15}$$

The inplane shear strain can then be easily computed by the third strain–displacement relation, namely,

$$\begin{aligned} \gamma_{xy}^0 &= \frac{\partial u^0}{\partial y} + \frac{\partial v^0}{\partial x} + \frac{\partial w^0}{\partial x}\frac{\partial w^0}{\partial y} \\ &= 2c_{12} + \left(c_9c_{10} - \frac{c_{11}^2}{4} + 2c_3 + 2c_6\right)xy + \left(\frac{1}{2}\left(\frac{c_9c_{11}}{2} + c_4\right) + c_{14}\right)x^2 + \left(\frac{1}{2}\left(\frac{c_{10}c_{11}}{2} + c_8\right) + c_{13}\right)y^2. \end{aligned} \tag{16}$$

This approach insures a consistent set of expressions for the needed midplane strains. None of the recent investigators (Jun and Hong, 1992; Peeters et al., 1996) studying more general unsymmetric laminates appeared to have taken this simple approach. The approximations obtained for the midplane strains use a total of 14 to-be-determined coefficients. Back-substituting the midplane strains and curvatures into the total strains, Eq. (4), and into the definition of the strain energy, Eq. (3), the spatial integrations in the expression for the strain energy can be conveniently carried out. The final result is an algebraic expression for the strain energy of the laminate of the form

$$\Pi = \Pi(c_i, i = 1, 14). \tag{17}$$

Obviously, Π is also a function of the laminate material properties, geometry, and temperature change, but here interest centers on its dependence on the unknown coefficients.

From Eq. (17), the first variation of the strain energy can be expressed as

$$\delta\Pi = \delta\Pi(c_1, c_2, \ldots, \delta c_1, \delta c_2 \ldots). \tag{18}$$

3.2. Formulating δW_F

Referring again to Fig. 2a and considering the laminate in a deformed configuration, the virtual work of the applied force $\underline{F}$ is defined as the work done by the force as the laminate is given a virtual displacement. The virtual displacement of the force is denoted as δR_F, as illustrated in Fig. 3. The figure represents half of the cross section of the laminate in the l–z plane, which is oriented at an angle β with the x-direction. The virtual displacement $\delta\underline{R}_F$ is not necessarily in the l–z plane. Similar effects occur at the other support. Note that during the virtual displacement the force remains parallel to the x–y plane. The total virtual work of the force $\underline{F}$ acting on the two supports can be expressed as,

$$\delta W_F = \vec{F} \cdot \delta\vec{R}_F\Big|_{\substack{x=L_s\cos\Phi_0 \\ y=L_s\sin\Phi_0}} + \vec{F} \cdot \delta\vec{R}_F\Big|_{\substack{x=-L_s\cos\Phi_0 \\ y=-L_s\sin\Phi_0}}. \tag{19}$$

The virtual displacement $\delta\vec{R}_F$ is evaluated by first computing the position vector $\vec{R}_F$ of the force relative to the origin of the coordinate system, then taking its variation. As illustrated in Fig. 4, the position vector R_F can be expressed as the sum of the position vector to the base of the support, $\vec{r}$, and the vector directed from the base of the support to the tip of the support, $\vec{n}^*$, i.e.,

$$\vec{R}_F = \vec{r} + \vec{n}^*. \tag{20}$$

The vector $\vec{r}$ can be written as

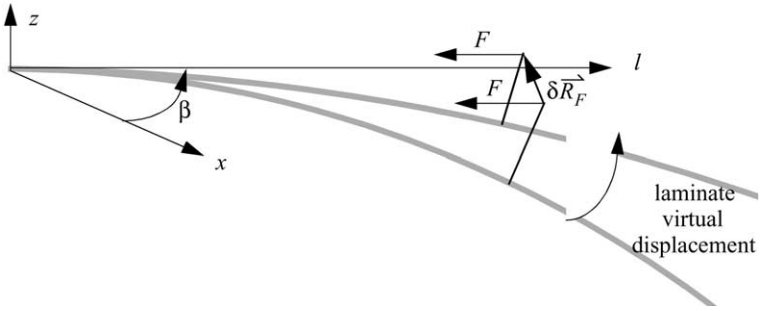

Fig. 3. Virtual displacement of the laminate.

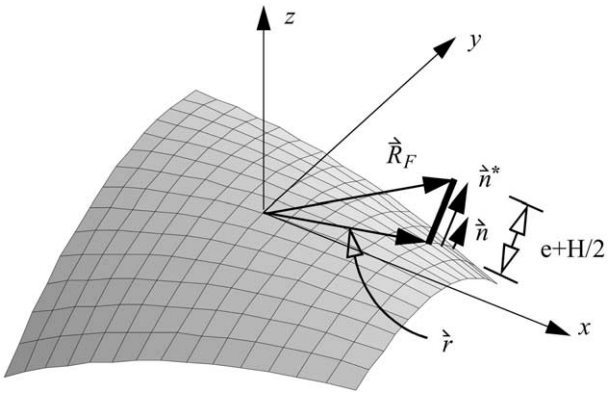

Fig. 4. Force position vector computation.

$$\vec{r} = (x + u^0(x, y, c_i, i = 1, 14))\vec{i} + (y + v^0(x, y, c_i, i = 1, 14))\vec{j} + w^0(x, y, c_i, i = 1, 14)\vec{k}, \tag{21}$$

where the notation is to emphasize the fact that the vector $\vec{r}$ depends on the unknown coefficients as well as x and y. Since the vector $\vec{n}^*$ is normal to the surface, it can be expressed as

$$\vec{n}^* = \left(e + \frac{H}{2}\right)\vec{n}, \tag{22}$$

where $\vec{n}$ is the unit vector normal to the laminate surface at the support locations ($x = \pm L_s \cos \Phi_0$, $y = \pm L_s \sin \Phi_0$) and $(e + H/2)$ is the distance from the laminate reference surface to the tip of the support. By definition, the unit vector $\vec{n}$ at a point (x, y) on the laminate surface is given by,

$$\vec{n}(x, y) = \frac{\frac{\partial \vec{r}}{\partial x} \times \frac{\partial \vec{r}}{\partial y}}{\left|\frac{\partial \vec{r}}{\partial x} \times \frac{\partial \vec{r}}{\partial y}\right|} = \frac{\overline{CP}}{|CP|}, \tag{23}$$

where the vectors $\partial\vec{r}/\partial x$ and $\partial\vec{r}/\partial y$ are tangent to the surface at point (x, y) and $\overline{CP}$ is shorthand for the cross product and expands to

$$\overline{CP} = CP_x\vec{i} + CP_y\vec{j} + CP_z\vec{k}, \tag{24}$$

with

$$|\overline{CP}| = \sqrt{CP_x^2 + CP_y^2 + CP_z^2}. \tag{25}$$

Using the definition of $\vec{r}$ given by Eq. (21) to compute the unit vector $\vec{n}$, vector $\vec{n}^*$ can then be computed. The virtual displacement δR_F is given by

$$\delta\vec{R}_F = \delta\vec{r} + \delta\vec{n}^*, \tag{26}$$

where from Eq. (21)

$$\delta\vec{r} = \sum_{i=1}^{14} \frac{\partial \vec{r}}{\partial c_i}\delta c_i \tag{27}$$

and from Eq. (22)

$$\delta\vec{n}^{*} = (e + H/2)\delta\vec{n}. \tag{28}$$

From Eqs. (23)–(25)

$$\delta\vec{n} = \frac{1}{|\overline{CP}|}\delta\overline{CP} + (-1)\frac{\overline{CP}}{|\overline{CP}|^2}\delta|\overline{CP}|, \tag{29}$$

or

$$\delta\vec{n} = \frac{1}{|\overline{CP}|}\left(\sum_{i=1}^{14}\frac{\partial\overline{CP}}{\partial c_i}\delta c_i\right) + (-1)\frac{\overline{CP}}{|\overline{CP}|^2}\left(\sum_{i=1}^{14}\frac{\partial\overline{CP}}{\partial c_i}\delta c_i\right). \tag{30}$$

Expanding, so the components of Eq. (30) are more completely understood, the derivative in the second summation is written out as

$$\frac{\partial|\overline{CP}|}{\partial c_i} = \frac{1}{2}\frac{\frac{\partial}{\partial c_i}(CP_x^2 + CP_y^2 + CP_z^2)}{\sqrt{CP_x^2 + CP_y^2 + CP_z^2}} = \frac{1}{2}\frac{\frac{\partial}{\partial c_i}(CP_x^2 + CP_y^2 + CP_z^2)}{|\overline{CP}|}. \tag{31}$$

With Eqs. (24), (25), and (31), Eq. (30) becomes

$$\delta\vec{n} = \sum_{i=1}^{14}\left(\frac{1}{|\overline{CP}|}\frac{\partial(CP_x\vec{i} + CP_y\vec{j} + CP_z\vec{k})}{\partial c_i} - \frac{1}{2}\left(\frac{\overline{CP}}{|\overline{CP}|^3}\right)\frac{\partial(CP_x^2 + CP_y^2 + CP_z^2)}{\partial c_i}\right)\delta c_i. \tag{32}$$

This expression is of the form

$$\delta\vec{n} = \sum_{i=1}^{14}\vec{N}_i\delta c_i, \tag{33}$$

where the definition of $\vec{N}_i$ is obvious and introduced as shorthand. As a result, using Eqs. (26)–(28), and (33), $\delta\vec{R}_F$ can be written as

$$\delta\vec{R}_F = \sum_{i=1}^{14}\left(\frac{\partial\vec{r}}{\partial c_i} + \left(e + \frac{H}{2}\right)\vec{N}_i\right)\delta c_i. \tag{34}$$

The applied force $\vec{F}$ can be expressed in terms of its components in the x–y–z coordinate system by

$$\begin{aligned}\vec{F}\Big|_{\substack{x=L_s\cos\Phi_0\\ y=L_s\sin\Phi_0}} &= (-F\cos\beta)\vec{i} + (-F\sin\beta)\vec{j},\\ \vec{F}\Big|_{\substack{x=-L_s\cos\Phi_0\\ y=-L_s\sin\Phi_0}} &= (F\cos\beta)\vec{i} + (F\sin\beta)\vec{j},\end{aligned} \tag{35}$$

where the $\cos\beta$ and $\sin\beta$ can be evaluated using the expression for $\vec{R}_F$ given by Eqs. (20)–(23). Specifically, letting $\vec{e}_l$ define the unit vector along the l-axis, then can $\vec{e}_l$ be expressed as a function of $\vec{R}_F$ by

$$\vec{e}_l = \frac{\vec{R}_F(x_s, y_s) - \vec{R}_F(-x_s, -y_s)}{|\vec{R}_F(x_s, y_s) - \vec{R}_F(-x_s, -y_s)|}, \tag{36}$$

where the vector defined by $\vec{R}_F(x_s, y_s) - \vec{R}_F(-x_s, -y_s)$ represents the vector pointing from the tip of the support at $(-L_s\cos\Phi_0, -L_s\sin\Phi_0)$ to the tip of support at $(L_s\cos\Phi_0, L_s\sin\Phi_0)$. The expressions for $\cos\beta$ and $\sin\beta$ needed in Eq. (35) can then be deduced from Eq. (36), since

$$\vec{e}_l = \frac{\vec{R}_F(x_s, y_s) - \vec{R}_F(-x_s, -y_s)}{|\vec{R}_F(x_s, y_s) - \vec{R}_F(-x_s, -y_s)|} = \cos\beta\,\vec{i} + \sin\beta\,\vec{j}. \tag{37}$$

By using Eqs. (35)–(37) to form the dot product of Eq. (19), the virtual work of the force δW_F can be computed.

3.3. Formulating δW_T

The principle of virtual work, Eq. (2), can now be expressed as

$$\begin{aligned}\delta W_{\mathrm{T}} &= \sum_{i=1}^{14} \frac{\partial \Pi}{\partial c_i}\delta c_i - \delta W_F \\ &= \sum_{i=1}^{14} f_i \delta c_i.\end{aligned} \tag{38}$$

The laminate is in equilibrium if the total virtual work vanishes, i.e., $\delta W_{\mathrm{T}} = 0$, for every admissible virtual displacement δc_i, $i = 1, 14$. Equating δW_{T} to zero results in

$$f_i = 0 \quad i = 1, 14, \tag{39}$$

which represent 14 highly nonlinear algebraic equations in the 14 unknown coefficients c_i, $i = 1, 14$. By setting the temperature change ΔT equal to $-280°\mathrm{F}$ and the force F to zero, solving the equilibrium equations expressed by Eq. (39) gives the cured shapes of the laminate at room temperature. By increasing F and keeping ΔT at $-280°\mathrm{F}$, the solutions of the equilibrium equations give the configurations of the laminate as it is deformed by the force F at room temperature. In the computation of the equilibrium solution using the Newton–Raphson technique, the Jacobian

$$J = \left[\frac{\partial f_i}{\partial c_j}\right] \quad i, j = 1, 14 \tag{40}$$

is computed for each temperature increment. The equilibrium solution is stable if and only if the matrix J is positive definite. By calculating the eigenvalues of the Jacobian matrix, the stability of the equilibrium solution can be assessed. When one eigenvalue is equal to zero or negative, the matrix is not positive definite and the equilibrium solution is unstable.

4. Numerical results

The 14 equilibrium equations given by Eq. (39) were solved for a number of laminates from three laminate families. The geometric and material properties of the laminates were chosen with consideration for the experimental work. Specifically, square eight-layer graphite-epoxy laminates 11.5×11.5 in.^{2} ($= L_x$ and L_y) and 0.040 in. thick ($= H$) were considered. The material properties of a layer of graphite-epoxy were assumed to be

$$\begin{aligned}&E_1 = 24.77 \times 10^6 \text{ psi} \quad E_2 = 1.27 \times 10^6 \text{ psi} \quad G_{12} = 1.03 \times 10^6 \text{ psi} \\ &v_{12} = 0.335 \quad \alpha_1 = 0.345 \times 10^{-6}/°\mathrm{F} \quad \alpha_2 = 15.34 \times 10^{-6}/°\mathrm{F}.\end{aligned} \tag{41}$$

It was assumed that the supports were attached 4 in. from the geometric center of the laminate (L_s of Fig. 2b equals 4.0 in.). The angle Φ_0 representing the principal curvature direction was determined from the calculations that led to figures like Fig. 5, to be discussed shortly, for each laminate. Obviously the length e

of the support was important, but for the present, only the moment will be considered. To obtain numerical results, the value of the applied moment was increased from zero to a level at which snap-through occurred. For every moment level, the equilibrium equations were solved, giving the curvatures κ_x^0, κ_y^0, and κ_{xy}^0 of the deformed laminate. From the values of these curvatures, the principal curvatures and principal curvature directions were computed as a function of the applied moment. In addition, the angle β was computed.

A comment is in order regarding the numerical solution of Eq. (39): In addition to appearing elsewhere, the unknown coefficients c_i, $i = 1, 14$ appear in the denominators of the equations of Eq. (39), due mainly to the form of Eq. (23). To make progress with the numerical computations, the force F was applied in small steps in an iterative fashion. For each increase in load, where a coefficient appeared in a denominator, the value from the previous iteration was used instead of treating it as an unknown. All these computations were performed using *Mathematica* (Wolfram, 1991).

4.1. Room-temperature configurations

Before discussing the snap-through behavior, to provide insight into the multiple laminate configurations at room temperature, it is worth discussing briefly the characteristics of the temperature–curvature relations for unsymmetric laminates. Fig. 5 shows the predicted temperature–curvature relations of unrestrained square 11.5×11.5 in.^{2} eight-layer $[90_4/0_4]_T$ and $[-60_4/30_4]_T$ laminates considered in the present study over the temperature range room temperature to cure temperature, the reference temperature ($\Delta T = 0°$) being the elevated cure temperature. Shown in the figure are the curvatures in the x- and y-directions, κ_x and κ_y, respectively, and the twist curvature, κ_{xy}, which is zero for the $[90_4/0_4]_T$ laminate. Considering a cooling scenario, the $[90_4/0_4]_T$ laminate starts flat at the cure temperature, point A in the figure. As the temperature is lowered, small curvatures develop. The curvatures are equal and opposite and thus the laminate deforms into a shallow saddle. At point B, about 25° below the cure temperature, the temperature–curvature relationships trifurcate and follow either paths BC, BE, or BD. With path BC the curvature in the x-direction increases while the curvature in the y-direction decreases. At room temperature, point C, the curvature in the x-direction dominates, resulting in the cylindrical configuration of Fig. 1b. With path BD the curvature in the y-direction increases while the curvature in the x-direction decreases. At room temperature, point D, the curvature in the y-direction dominates, resulting in the cylindrical configuration of Fig. 1c. With path BE the curvatures increase slightly and remain equal in magnitude but opposite in sign. Point E corresponds to the saddle configuration of Fig. 1d. A stability analysis indicates that path BE is unstable and paths BC and BD are stable. The results for the $[-60_4/30_4]_T$ laminate are similar, except for the existence of a twist curvature. The various shapes for the $[-60_4/30_4]_T$ laminate are shown in the right-hand portion of Fig. 5.

4.2. Snap-through behavior

The deformation and snap-through behavior of the laminates from the $[(\Theta - 90)_4/\Theta_4]_T$ family, $\Theta = 0°$, 15°, and 30°, is illustrated in Fig. 6 by way of moment vs. curvature relations. When no moment is applied it is assumed the initial shapes of the laminates are cylindrical with large principal curvature K_1 and small principal curvature K_2. This corresponds to point C in the three parts of Fig. 5, which shows the cases for $\Theta = 0°$ and 30° from this laminate family. (Points C, D, and E in Fig. 6 are the same as denoted in Fig. 5.) As has been discussed, for the zero applied moment condition, the equilibrium equations have two other solutions for the laminate configuration. One corresponds to the unstable configuration, point E, and the other corresponds to the second stable cylindrical configuration, point D. As the moment is increased, the curvature K_1 decreases and curvature K_2 remains imperceptibly small. When the moment is large enough, point G in the figure, the laminates reach an unstable configuration and snap into the other cylindrical

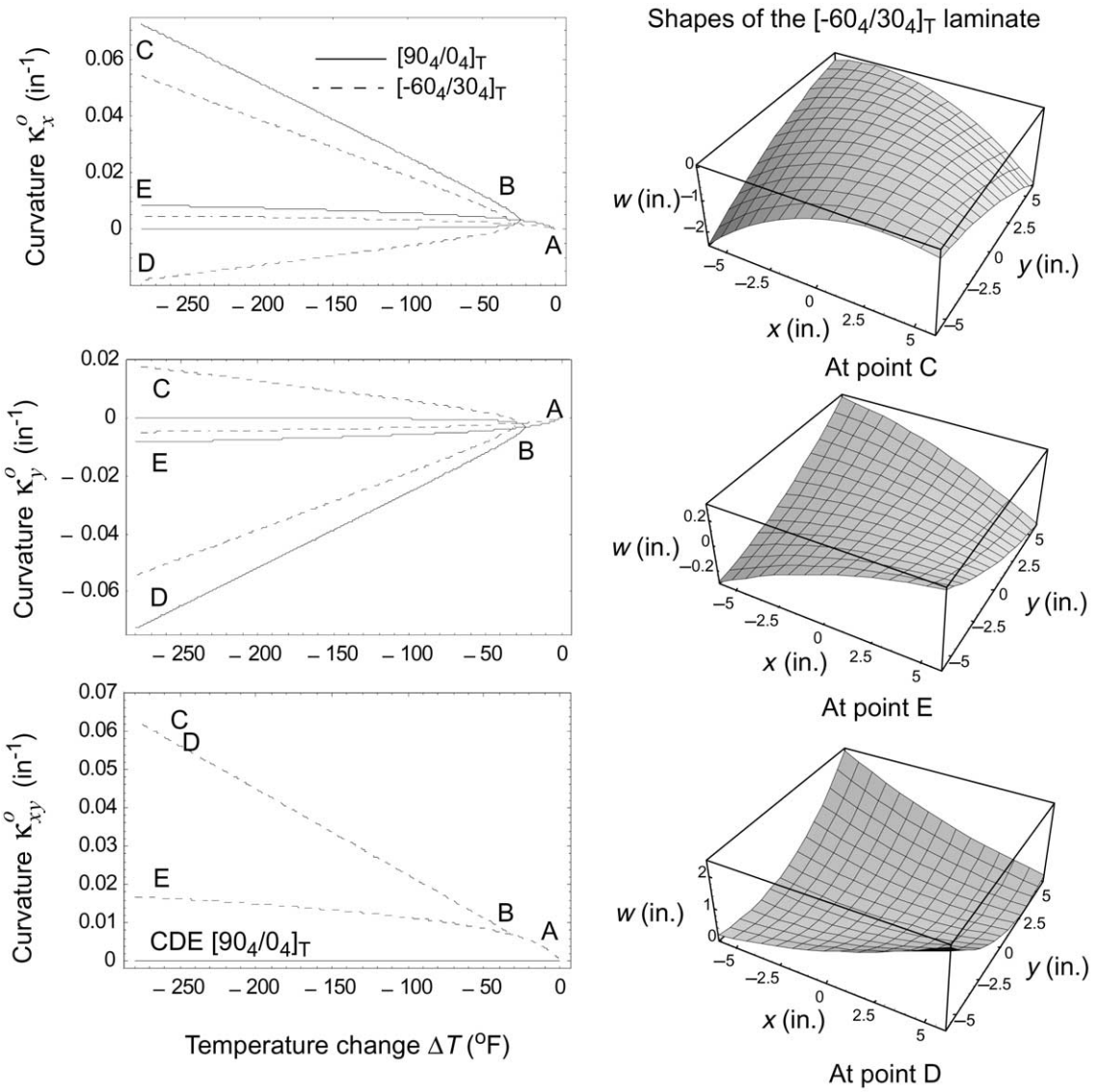

Fig. 5. Temperature–curvature relations for $[(\Theta - 90)_4/\Theta_4]_T$ laminates.

shape. The snap-through is indicated by the arrow from G to D′ and is due to K_1 becoming a small positive quantity and K_2 becoming a large negative quantity. As can be noted in the bottom portion of Fig. 6, during the application of the moment, the principal curvature direction Φ does not change relative to its value for the no-moment condition, Φ_0. Additionally, the angle β (not shown) remains equal to $\Phi(=\Phi_0)$. The moment–curvature relation does not depend strongly on the fiber direction Θ.

The moment–curvature relations for the $[(90 - \Theta)_4/\Theta_4]_T$ family are featured in Fig. 7. It is seen that for this family the snapping moment is highly dependent on the fiber orientation. As the angle between the two fiber orientations decreases, the moment required for snapping decreases. Unlike the first family, the principal curvature direction depends strongly on the applied moment level, and the principal curvature

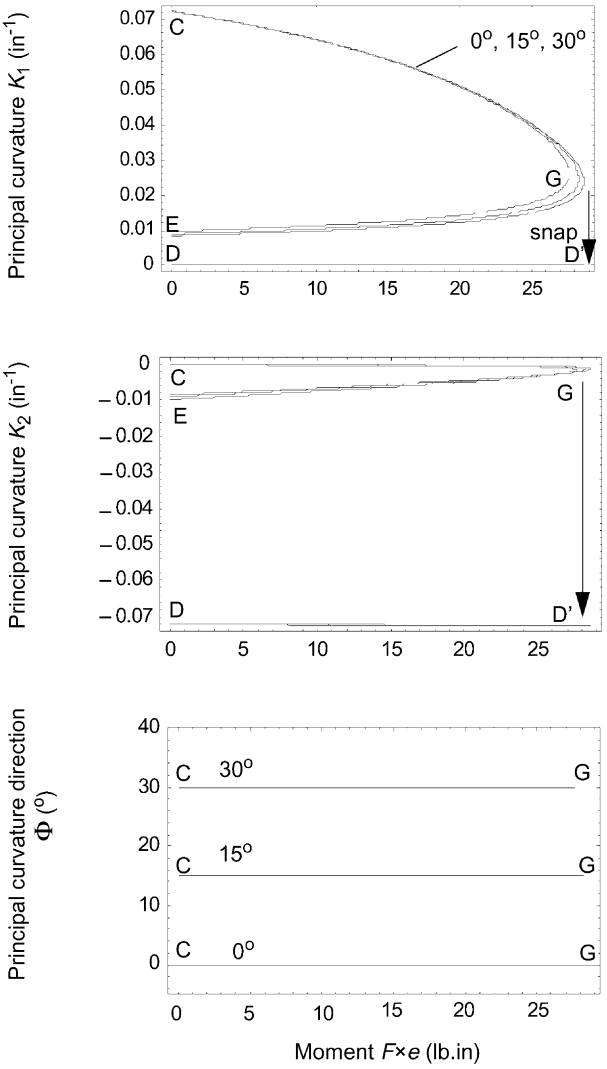

Fig. 6. Moment–curvature relations for $[(\Theta - 90)_4/\Theta_4]_T$ laminates.

directions appear to be zero at the snapping moment. The numerical solution scheme is somewhat erratic at the snap-through condition, so the solution exactly at the snap-through condition has not converged as well as at other moment levels. More will be said of this shortly. The angle β (not shown), which at the no-force condition is equal to Φ_0, changes very little (less than a degree) for all force levels. For laminates of the $[-\Theta_4/\Theta_4]_T$ family shown in Fig. 8, the magnitude of the snapping moment also depends strongly on the fiber orientation. The principal curvature direction depends strongly on the level of applied moment. The angle β (not shown), however, remains virtually unchanged with force level. For this family, the principal curvature direction appears to be 45° at snap-through.

As can be seen, there is a variety of snapping moment levels and changes in principal curvature directions among these three families of laminates. The behavior of the principal curvature direction with increasing moment for the three families is an important aspect of the snap-through phenomenon. For each

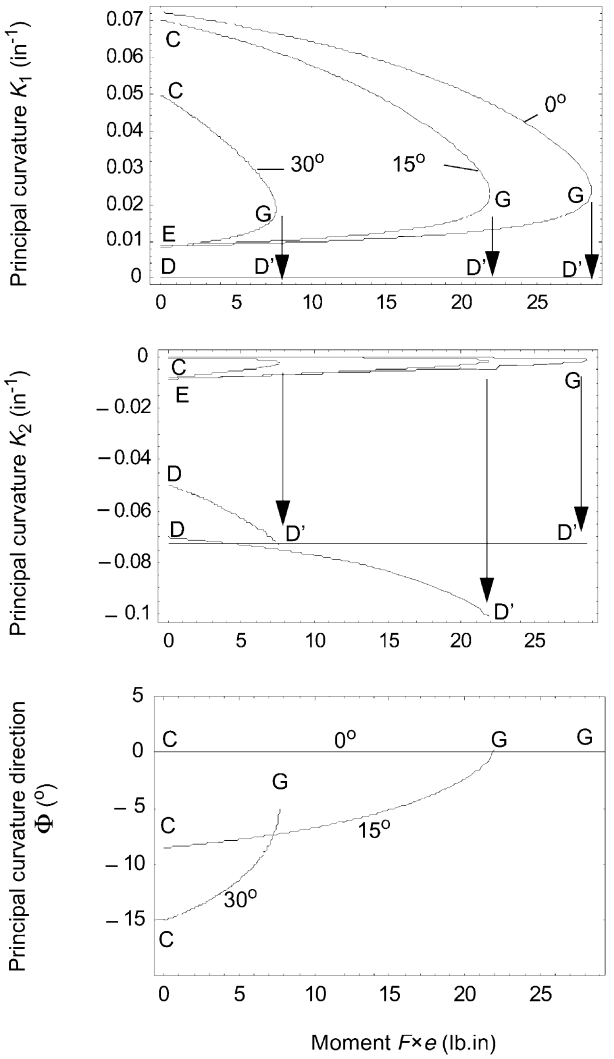

Fig. 7. Moment–curvature relations for $[(90-\Theta)_4/\Theta_4]_T$ laminates.

laminate in the $[(\Theta-90)_4/\Theta_4]_T$ family, the principal curvature direction of the unstable saddle configuration is the same as the principal curvature direction associated with major curvature K_1 of the one of the two stable cylindrical configurations. For each laminate of the $[(90-\Theta)_4/\Theta_4]_T$ family, the principal curvature direction of the unstable saddle configuration is 0°. For each laminate of the $[-\Theta_4/\Theta_4]_T$ family, the principal curvature direction of the unstable saddle configuration is 45°. It is apparent that as the stable cylindrical configuration with curvature K_1 is flattened by increasing levels of the applied moment, the principal curvature direction of the flattened configuration approaches that of the room-temperature saddle configuration, and when the flattened configuration becomes unstable, the principal curvature direction coincides with that of the unstable saddle. As snap-through is a dynamic event and the present analysis is static, it is only possible to conjecture as to the meaning of this observation. One possibility is that when passing from one stable cylindrical configuration to the other, for a brief instant the laminate assumes the unstable saddle configuration.

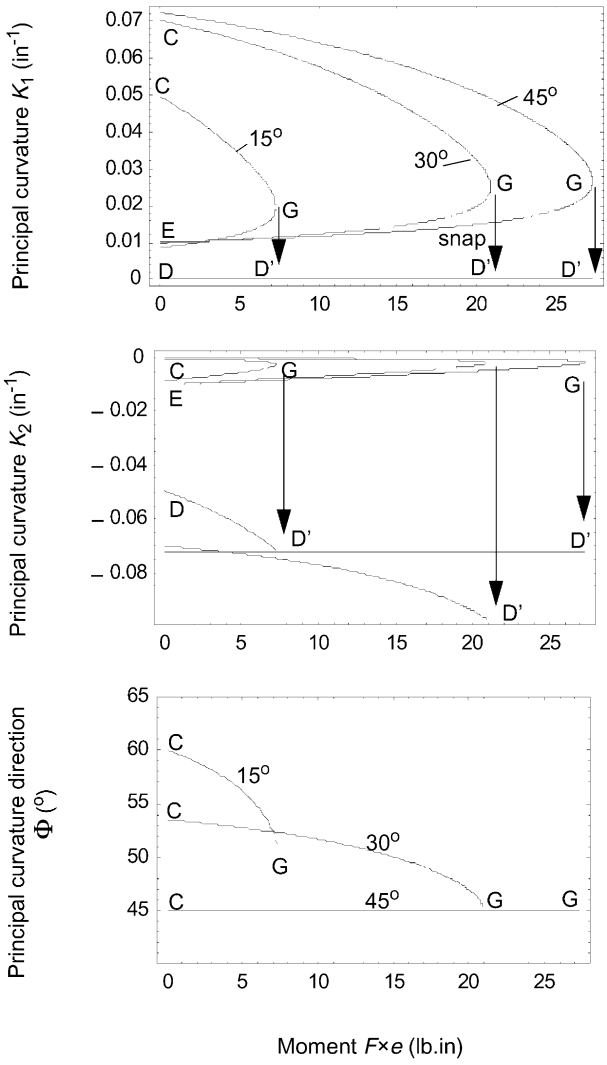

Fig. 8. Moment–curvature relations for $[-\Theta_4/\Theta_4]_T$ laminates.

5. Experimental set-up

To determine the degree to which the numerical predictions were accurate, a number of eight-layer unsymmetric graphite-epoxy laminates were fabricated. The laminates were 0.040 in. thick and square and were trimmed to have a side length of 11.5 in., the dimensions used to obtain numerical results in the last section. As graphite-epoxy is dark in color, before curing the laminates at an elevated temperature, lighter color Kevlar fibers were laid at intervals in the x- and y- directions to form a grid to make it easier to see the deformations of the laminates. The laminates were loaded with a rather simple loading scheme that used water filling a container to apply an ever-increasing tension level to a thin wire that was attached to supports which, in turn, were attached to the laminate. The loading scheme was designed to assure that the laminates were being loaded in a force-control mode that was not contaminated by any restraint on dis-

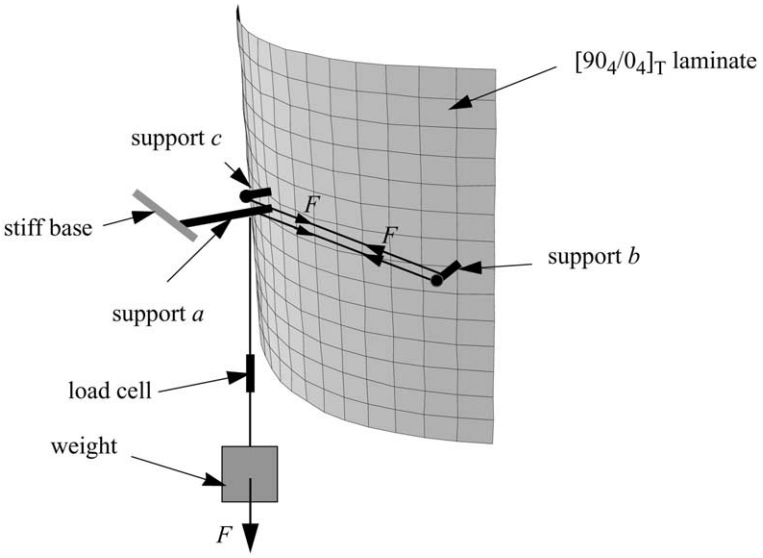

Fig. 9. Description of experimental set-up.

placements. A schematic of the loading arrangement, showing a $[90_4/0_4]_T$ laminate, is illustrated in Fig. 9. Three supports, labeled a, b, and c in the figure, were attached to the laminate by bolts through holes drilled through the laminates. Support a was longer than supports b and c and served the dual role of applying force to the laminate and attaching the laminate/forcing system to a stiff base. The end of a thin wire was fixed at support c and was looped half-way around support b, then back to support a. At each support the wire was a known distance from the midplane of the laminate, providing a known moment arm through which the force acted to produce a moment. Specifically, e in Figs. 2 and 4 and Eq. (34) was 0.625 in. The wire was looped quarter-way around support a and then down to a load cell, which was attached in series to a water container. With this looped wire arrangement, the laminate was subjected to twice the force level registered by the load cell. Due to the deformation of the laminate as the force level was increased, the thin wire actually had to slide slightly around supports b and a. Care was taken to ensure that this slippage could occur with minimal friction. Though curvatures have been discussed to this point, it is difficult to measure them directly. Since the primary interest in this work was the determination of the snap-through force level, back-to-back strain gage rosettes were used to monitor the response of the laminate as a function of force. The load cell and strain gage signals were recorded by a computer. Fig. 10 is a photograph of a $[-30_4/30_4]_T$ laminate being loaded. The lighter color Kevlar grid on the plate can be seen, as can the three supports, C-clamps for clamping the plate to the stiff base using the longer support, and the strain gage leads. The experimental procedure was as follows: The laminate, with the three supports attached, was clamped into position, as in Figs. 9 and 10. With the load cell monitoring the tension in the wire, and the strains being recorded, water was slowly added to the container by way of a small-diameter tube. At snap-through the strains experienced a large change in value. By examining the resulting force–strain data, the force at snap-though could be determined. Actually, water flow was stopped at snap-through and the weight of water was used as another measure of the snap-through force. By carefully watching the laminate, it was possible to anticipate the snap-through event and terminate the water flow without any danger of overfilling the water container. Of course with the load cell and water container adding to the tension in the wire, these effects had to be accounted for. As an additional step, each laminate was loaded and the snap-through event recorded at least twice.

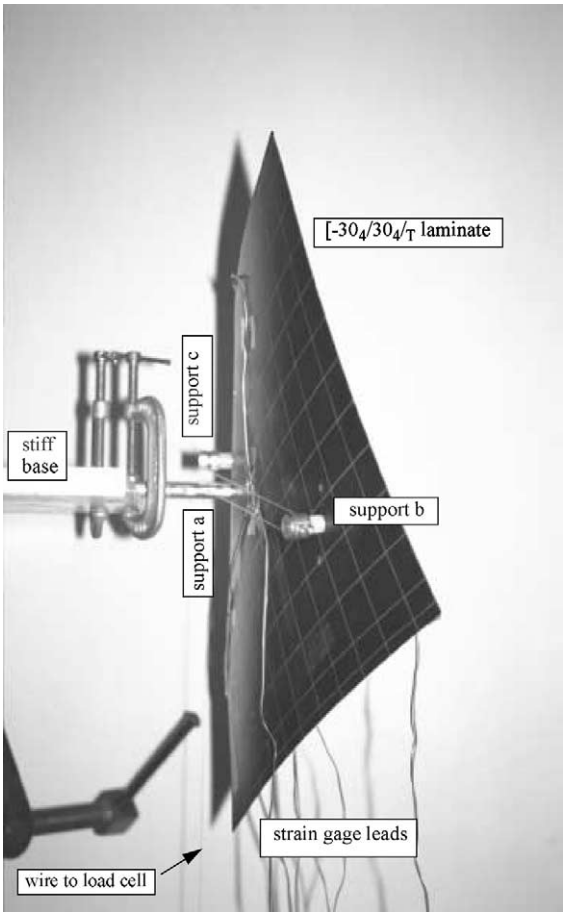

Fig. 10. Photograph of experimental set-up.

6. Comparison of numerical results with experiments

The loading apparatus described in the last section was used to load four laminates. The specific layups were: $[90_4/0_4]_T$, a member of several families and shown in Fig. 6; $[-60_4/30_4]_T$, a member of the $[(\Theta - 90)_4/\Theta_4]_T$ family and shown in Fig. 6; $[60_4/30_4]_T$, a member of the $[(90 - \Theta)_4/\Theta_4]_T$ family and shown in Fig. 7; $[-30_4/30_4]_T$, a member of the $[-\Theta_4/\Theta_4]_T$ family and shown in Fig. 8. The developed theory was used to predict the snap-through force for these laminates, namely point G on Figs. 6–8. The results are summarized in Table 1.

The calculation of the theoretical value of forces needs to be explained. To predict the shape of the laminate before any force was applied, it was initially assumed that the shape was the result of a $-280°$F temperature change relative to the cure temperature. Specifically, it was assumed that the cure temperature was 350°F and the cooled temperature was 70°F. As was discussed in Dano and Hyer (1997), when using this $-280°$F temperature change, the measured curvatures were generally less than the predicted curvatures. This could easily be the case if the stress-free temperature of the laminate was less than 350°F, or if there were polymer matrix shrinkage effects. However, it was also noted that when the curvatures were measured six months later, they were less than the first measurement. This was attributed to relaxation effects in the

Table 1
Comparison between theory and experiments of snap-through forces

Laminate	From strain gage data (lb)			From weight of water (lb)			Theory (lb)
	Test 1	Test 2	Test 3	Test 1	Test 2	Test 3	
$[90_4/0_4]_T$	18.14	16.39	–[a]	16.99	15.43	–[a]	17.10
$[-60_4/30_4]_T$	–[b]	13.48	13.33	–[b]	13.16	13.02	14.10
$[60_4/30_4]_T$	3.59	3.33	3.13	3.93	4.14	4.01	3.30
$[-30_4/30_4]_T$	9.23	9.55	9.34	8.89	8.69	8.49	11.95

[a] Test 3 not conducted.
[b] Wire broke near maximum load.

polymer matrix, as drying the laminates had no influence on the curvatures. Hence, to compute the predicted snap-through force in Table 1, the curvature just before the load was applied was used as the starting point, not the curvature corresponding to a −280°F temperature change. This pre-loading curvature was predicted by using a stress-free temperature lower than 350°F. With that in mind, it is seen that the

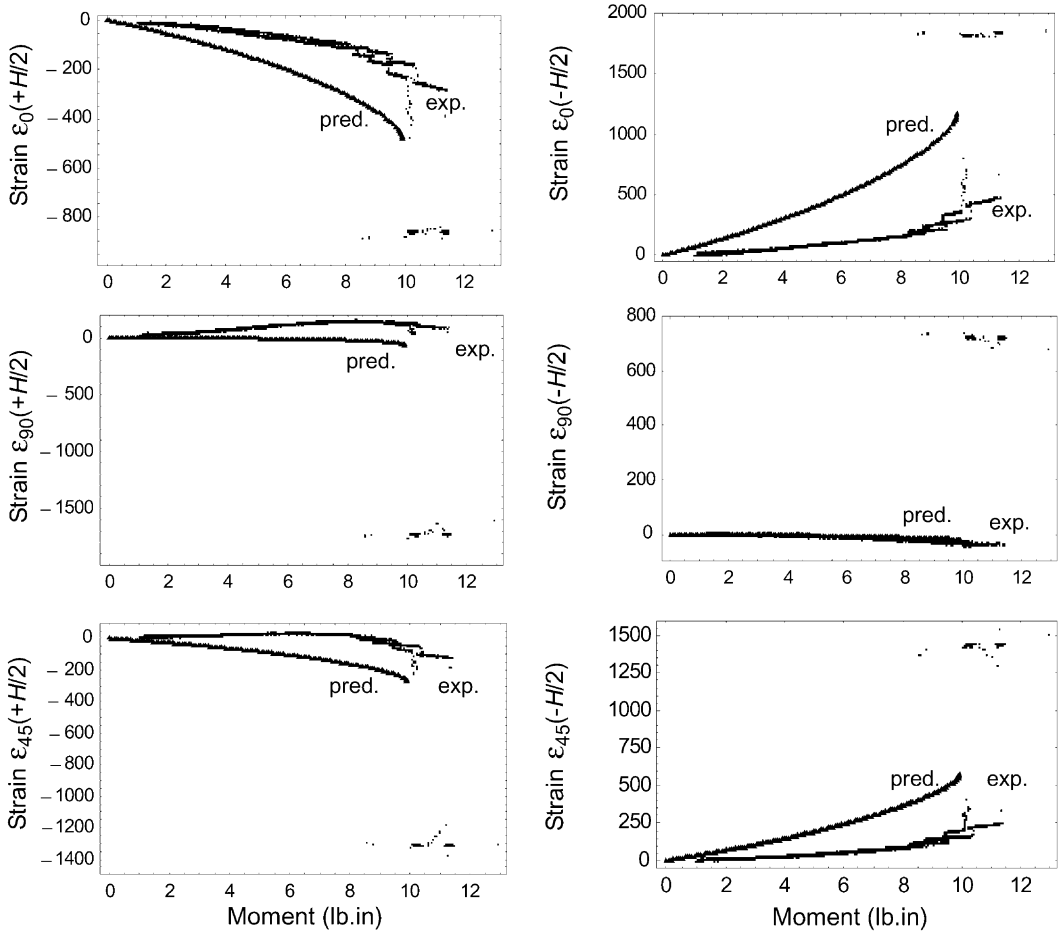

Fig. 11. Experimentally and predicted moment–strain relations for the $[90_4/0_4]_T$ laminate.

comparison between predicted and measured snap-through force levels is reasonable. Within the experiments, for a given laminate, there is scatter to the results. Within the strain gage measurements, there is about a 15% spread (for the $[60_4/30_4]_T$ laminate) and within the water weight measurement, there is up to a 10% spread (for the $[90_4/0_4]_T$ laminate). Moreover there is a noticeable difference between the strain gage measurement and the water weight measurement. A re-examination of the experimental procedure and raw data has not provided an explanation. However, the results in Table 1 verify that the predictions and experiments are in good qualitative agreement, and the quantitative comparison is also quite reasonable. Specifically, the data in Table 1 confirm the prediction that the snapping force level is proportional to the angle between the two fiber directions, the 30° difference of the $[60_4/30_4]_T$ case resulting in the least force required for snapping. Unfortunately, since the relaxation effects were not the same in each laminate, it was not possible to verify that the snap-through moment levels in the $[90_4/0_4]_T$ and $[-60_4/30_4]_T$ laminates were identical, as Fig. 6 predicts.

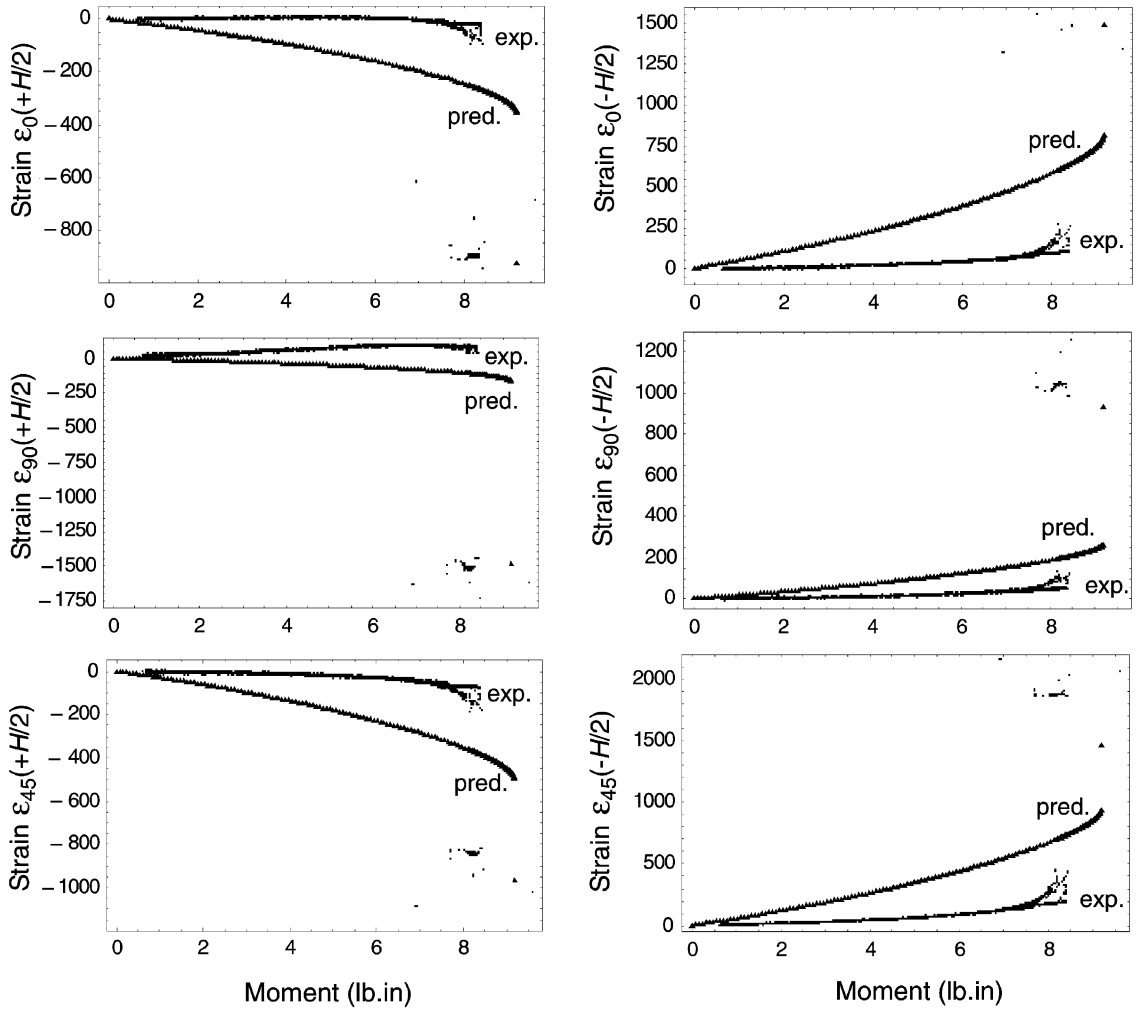

Fig. 12. Experimental and predicted moment–strain relations for the $[-60_4/30_4]_T$ laminate.

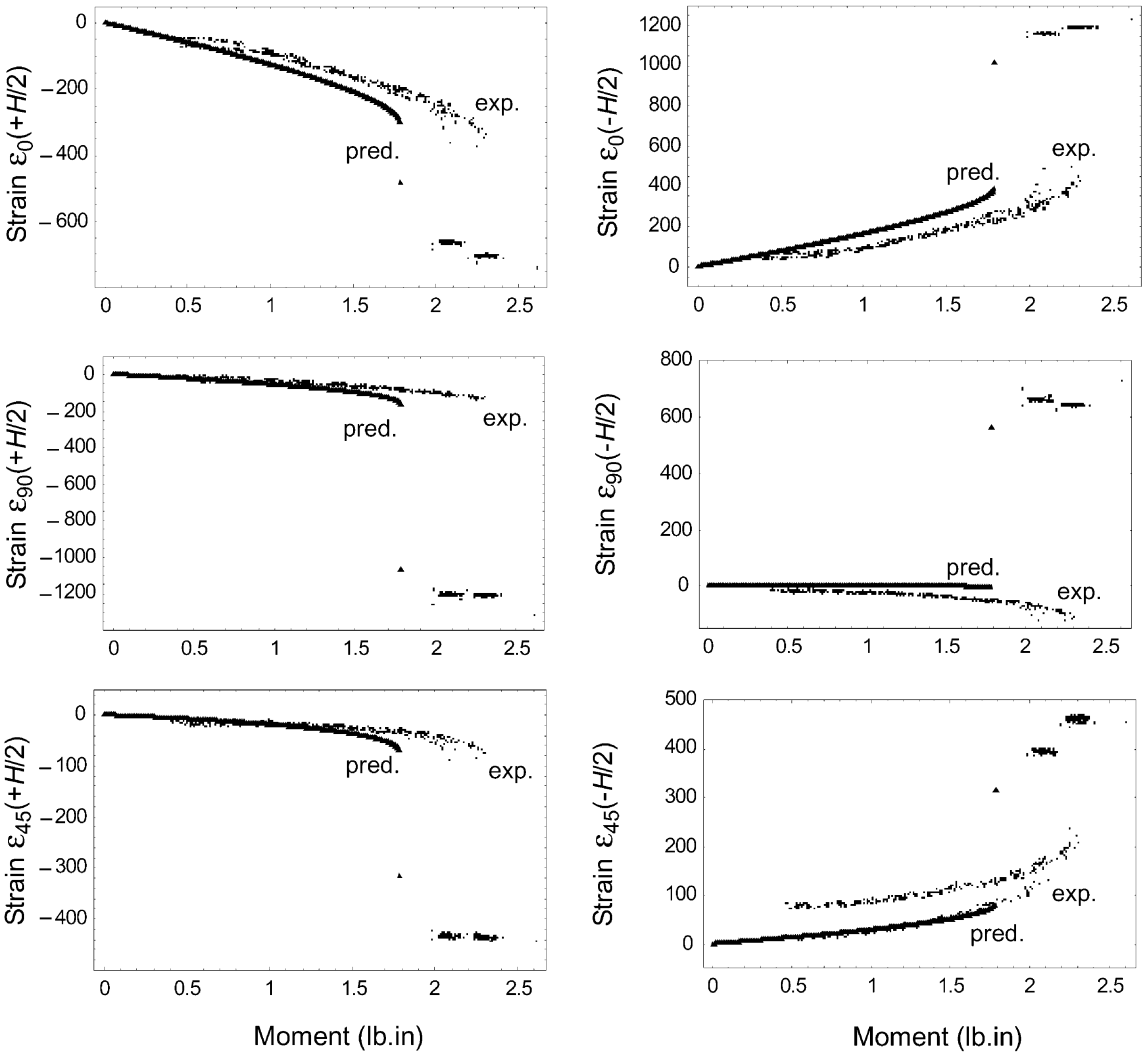

Fig. 13. Experimental and predicted moment–strain relations for the $[60_4/30_4]_T$ laminate.

Figs. 11–14 provide another comparison between predictions and experiments. These figures illustrate the relations between the strains along the 0°, 90° and 45° directions, and the applied force as measured by the strain gages at the center of each panel. Since data were sampled at discrete times by the data acquisition system, the experimental relations consist of points rather than a continuous curve. The notation '$+H/2$' and '$-H/2$' simply refers to which side of the laminate the gage was on. On each figure are the multiple strain traces, corresponding to the multiple tests, along with a single trace that is the prediction. The data point at the beginning of the discontinuity in each trace of experimental data was used as the indicator of snap-through for that test. These are the data used in Table 1. After the beginning of the snap-through event, the measured strains are not considered meaningful since the event, as mentioned before, is dynamic and there was flexural motion of the panel.

From the four figures several points are evident. First, for all laminates and all repeated tests the snap-through event is distinct and can be easily determined from the strain vs. force traces. Also, in the context of

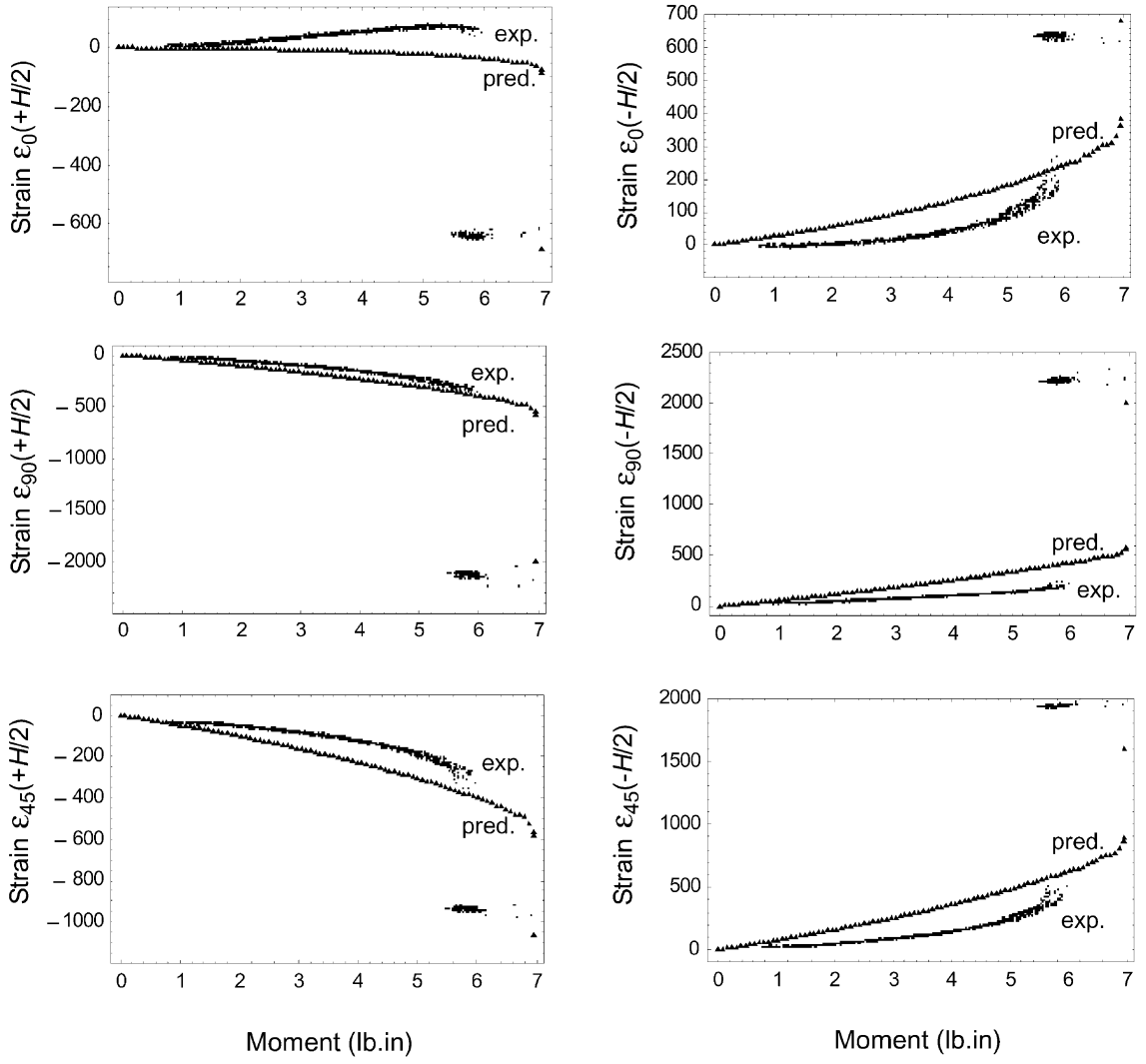

Fig. 14. Experimental and predicted moment–strain relations for the $[-30_4/30_4]_T$ laminate.

Table 1, the experimental results are reasonably repeatable. Second, the difference between the predicted and measured strain magnitudes are most noticeable for the $[90_4/0_4]_T$ and the $[-60_4/30_4]_T$ cases, the stiffest laminates, the two fiber angles within the laminate being 90° apart. Local deformations in the laminates at the base of the supports not accounted for in the analysis, which is a global-level analysis – i.e., it is based on the assumption that curvatures c_9, c_{10}, and c_{11} in Eq. (8) are valid throughout the laminate – are most likely responsible for the deviations in these stiffer laminates. The forces actually cause the laminate to deform locally at the base of the supports rather than deform more uniformly over the entire laminate, so there is not as much strain produced away from the supports where the strain gages are mounted as there is near the supports. Finally, it should be noted that the front and back strain levels are not equal and opposite, as might be expected in a bending problem. The presence of the bending-extension coupling effects inherent with unsymmetric laminates are responsible for this.

7. Summary and conclusions

Presented has been an approximate theory developed to predict the snap-through event in generally unsymmetric laminates. Though the event is a dynamic one, a static approach has been taken. The theory is based on assumed forms for the inplane strain and out-of-plane displacement fields, and uses the Rayleigh–Ritz technique and virtual work. Numerical predictions were presented for three specific families of laminates. It was shown that the snapping moment (force) levels for these families depends on the angle between the two fiber directions characteristic of these laminates. A simple experimental set-up, designed to measure the snapping force levels and strains in selected laminates, was described. Comparisons between predictions and experimental results were good. Because of polymer relaxation effects, however, it was not possible to compare all aspects of the experiments with predictions. None-the-less, it can be concluded that the theory presented is accurate enough that it can be used with confidence to move on to employing active SMA wires, for example, to develop the necessary forces. The issues with that approach are the generation of sufficient force levels, while staying within the strain constraints of those materials, and initiating the phase transformation.

Acknowledgements

Both authors wish to express their appreciation for the partial support of grant NAG-1-343, the NASA-Virginia Tech Composites Program, from the Mechanics and Durability Branch of the NASA Langley Research Center. Also, support from the Center for Composite Materials and Structures at Virginia Tech is appreciated.

References

Cho, M., Kim, M.-H., Choi, H.S., Chung, H.C., Ahn, K.-J., Eom, Y.S., 1998. A study on the room-temperature curvature shapes of unsymmetric laminates including edge effects. J. Compos. Mater. 32 (5), 460–482.

Dang, J., Tang, Y., 1986. Calculation of the room-temperature shapes of unsymmetric laminates. Proceedings of International Symposium on Composite Materials and Structures, available Technomic Publishing Co. Inc., Lancaster, PA, pp. 201–206.

Dano, M.-L., Hyer, M.W., 1996. The response of unsymmetric laminates to simple applied forces. Mech. Compos. Mater. Struct. 3, 65–80.

Dano, M.-L., Hyer, M.W., 1997. Thermally-induced deformation behavior of unsymmetric laminates. Int. J. Solids Struct. 35 (17), 2101–2120.

Hamamoto, A., Hyer, M.W., 1987. Non-linear temperature–curvature relationships for unsymmetric graphite epoxy laminates. Int. J. Solids Struct. 23 (7), 919–935.

Hyer, M.W., 1981a. Some observations on the cured shapes of thin unsymmetric laminates. J. Compos. Mater. 15, 175–194.

Hyer, M.W., 1981b. Calculations of the room-temperature shapes of unsymmetric laminates. J. Compos. Mater. 15, 296–310.

Hyer, M.W., 1982. The room-temperature shapes of four-layer unsymmetric cross-ply laminates. J. Compos. Mater. 16, 318–340.

Hyer, M.W., 1998. Stress analysis of fiber-reinforced composite materials. WCB/McGraw-Hill, New York.

Jun, W.J., Hong, C.S., 1990. Effect of residual shear strain on the cured shape of unsymmetric cross-ply thin laminates. J. Compos. Sci. Technol. 38, 55–67.

Jun, W.J., Hong, C.S., 1992. Cured shape of unsymmetric laminates with arbitrary lay-up angles. J. Reinforced Plastics Compos. 11 (12), 1352–1366.

Peeters, L.J.B., Powell, P.C., Warnet, L., 1996. Thermally-induced shapes of unsymmetric laminates. J. Compos. Mater. 30 (5), 603–626.

Schlecht, M., Schulte, K., Hyer, M.W., 1995. Advanced calculations of the room-temperature shapes of thin unsymmetric composite laminates. Compos. Struct. 32, 627–633.

Schlecht, M., Schulte, K., 1999. Advanced calculations of the room-temperature shapes of unsymmetric laminates. J. Compos. Mater. 33 (16), 1472–1490.

Tuttle, M.E., Koehler, R.T., Keren, D., 1996. Controlling thermal stresses in composites by means of fiber prestress. J. Compos. Mater. 30 (4), 486–502.

Wolfram, S., 1991. Mathematica: A System for Doing Mathematics by Computer. Addison-Wesley Publishing Co., Redwood City, CA.